Interstitial migration in irradiated iron and iron-based dilute alloys. I. Interstitial trapping and detrapping in FeMo, FeV and FeTi dilute alloys



1990 J. Phys.: Condens. Matter 2 9269

(http://iopscience.iop.org/0953-8984/2/47/004)

J. Phys.: Condens. Matter 2 (1990) 9269–9290. Printed in the UK

# Interstitial migration in irradiated iron and iron-based dilute alloys: I. Interstitial trapping and detrapping in FeMo, FeV and FeTi dilute alloys

F Maury†, A Lucasson, P Lucasson, P Moser‡ and F Faudot§
UA CNRS No 803, Université Paris XI, F-91405 Orsay, France

Received 17 July 1989, in final form 8 February 1990

**Abstract.** Three series of dilute iron alloys, with oversized solutes, **Fe**Ti, **Fe**V and **Fe**Mo, in the concentration range 50 at.ppm to 3 at.%, have been electron-irradiated at low temperature together with the metal. A strong dependence of the solute and defect resistivities on the solute concentration is observed, which is analysed in terms of the two-current model. The specimens have then been annealed throughout stage I (self-interstitial migration) and stage II up to stage III (vacancy migration), with their resistivity measured. In these alloys, the mobile Fe self-interstitials, which are not annihilated at vacancies, are observed to get trapped at solute atoms in stage I and released from traps in stage II. Detrapping occurs in stage II at a temperature, $T_{II}$, depending on the solute. Trapping is the weakest for V ($T_{II} \simeq$ 140 K) and the strongest for Ti ($T_{II} \simeq$ 180 K). At very low concentration (50 and 100 at.ppm), the solute trapping efficiency is lost at the beginning of stage III (200 K) for all these solutes. In the most concentrated **Fe**Mo alloys, an important fraction of the radiation-induced resistivity is retained at 200 K, due to multiple trapping (trapping of iron interstitials by more than one Mo atom).

## 1. Introduction

The damage pattern of an irradiated alloy depends on the respective mobilities of the radiation-induced defects, interstitials and vacancies, at the irradiation temperature. It has been observed for example, in dilute **Ag**Zn alloys, that when the solute concentration is increased beyond a few per cent, the interstitials are slowed down so much, due to multiple trapping, that voids are created instead of the dislocation loops that form in very dilute alloys (Régnier and Halbwachs 1980).

On the other hand, in BCC alloys, solute long-range diffusion is expected to occur already at low temperatures with a high efficiency through mixed-interstitial long-range migration (Lucasson *et al* 1985). According to a simple model, which assumes that the size parameter is the decisive parameter for the formation of mixed interstitials (Dederichs *et al* 1978), mixed interstitials should not be formed with 'oversized' solutes. Yet channelling experiments have shown that mixed interstitials are indeed able to form with slightly oversized solutes such as Ag, Ga, Ge in Al (Swanson *et al* 1980). In these three cases, the impurity size effect is small: the Pauling metallic radius of the solute

† Present address: Laboratoire des Solides Irradiés, Ecole Polytechnique, F-91128 Palaiseau Cédex, France.
‡ CEN G-DRF-SPh MP, 85 X, F-38041 Grenoble Cédex, France.
§ CECM, 15 rue G Urbain, F-94407 Vitry, France.

0953-8984/90/479269 + 22 $03.50 

(Taylor 1961) is not larger than that of the solvent by more than 1% ($\Delta R/R \leqslant 1\%$). No mixed interstitials have been observed with more oversized solutes such as Mg, In, Sn in Al or Ag, Sb, Au in Cu or Te, Au in Fe (Swanson *et al* 1980), for which $\Delta R/R > 10\%$.

As a step towards a deeper insight into the influence of various parameters such as solute size effect, electron concentration, etc., on the behaviour of irradiated dilute iron alloys, which could lead to a better understanding of the behaviour of irradiated commercial steels, we have investigated a number of metallic solutes in $\alpha$-iron, which enter the composition of commercial low-alloy ferritic steels. The present paper deals with the three 'oversized' solutes: Mo, V and Ti. Results obtained with Mn, Ni and Cu are reported in the following paper. Other results obtained with Si (Maury *et al* 1985), Co (Maury *et al* 1986) and Cr (Maury *et al* 1987) have already been reported.

In section 2, we briefly describe the specimen characteristics and experimental conditions. In section 3, we discuss the interpretation of the resistivity measurements in the particular case of Fe and Fe alloys. In sections 4, 5, 6 and 7, we analyse the stage I and stage II recovery spectra of Fe, **Fe**Mo, **Fe**Ti and **Fe**V.

## 2. Experimental specifications

The pure iron and the alloys were prepared in Grenoble (CENG) except for two **Fe**Ni alloys prepared in Vitry (CECM). The **Fe**Ti, **Fe**Cu and **Fe**V alloys were cold-rolled in Grenoble to a thickness of about 100 $\mu$m. The samples ($\simeq 1 \times 25\ mm^2$) were then chemically thinned in a $H_2O_2$ (95%) + HF (5%) bath. The **Fe**Mn, **Fe**Ni and **Fe**Mo alloys were cold-rolled in Vitry directly to a thickness of about 50 $\mu$m. This procedure results in a better definition of the sample thickness but, in case of surface contamination during the alloy elaboration, may lead to poorer purity. Before mounting, the samples were annealed in hydrogen: 3 or 4 h at 730 °C or, for a few of them, 24 h at 850 °C.

The main residual impurity is Si (a few to 30 at.ppm); the concentration of all other elements (H, C, N, O, Al, . . .) is $\leqslant 1$ at.ppm in the purest samples and may reach a few ppm (Ni, Cu, . . .) in the less pure ones. The grain size is $\simeq 0.5$ to 1 mm (Vanoni 1973).

The specimen characteristics for the alloys **Fe**Mo, **Fe**V and **Fe**Ti are listed in table 1.

The sample thickness was measured with a micrometer. The shape factor of the samples was deduced from geometry and, for the most dilute alloys, from their room-temperature resistance. Both determinations agreed within less than 10%.

The samples were irradiated with 1.6 MeV electrons in Orsay, up to a fluence of $7.4 \times 10^{17}\ e^-/cm^2$. Their temperature during the irradiation (25 to 35 K) was controlled by recording their electrical resistivity. The resistivity measurements were performed at liquid-helium temperature without a magnetic field. The fluctuations of the irradiation temperature from one sample to another mainly reflect the beam inhomogeneity. The uncertainty on the radiation-induced resistivity comes both from the beam inhomogeneity and from the uncertainty on the shape factor. For the most concentrated alloys, the shape factor is measured geometrically and the corresponding uncertainty on the radiation-induced resistivity, as well as on the specific solute resistivity, is $\leqslant 10\%$.

## 3. Solute and defect specific resistivity

### *3.1. Solute resistivity*

The apparent solute specific resistivity is defined as

**Table 1.** Specimen characteristics.

| Alloy and sample number[a] | Sample mean thickness ($\mu$m) | Solute concentration, $c_s$ | Residual resistivity, $\rho_0 \equiv \rho_{4K}$ (n$\Omega$ cm) | Apparent solute specific resistivity, $\rho_s^*$ ($\mu\Omega$ cm) | Solute specific resistivity from literature[b] ($\mu\Omega$ cm) | Irradiation conditions: dose ($e^-/cm^2$) and temperature (K) | Radiation-induced resistivity, $\Delta\rho_0$ (n$\Omega$ cm) |
|---|---|---|---|---|---|---|---|
| **Fe**Ti | | | | | | $6.3 \times 10^{17}$ | |
| 1.1 | ≃27 | 0 | 33 | — | 255[1] | 20 | 62–58–59 |
| | | | | | 300[2] | 117 | 21[c] |
| | | | | | 290[3] | 134 | 16[c] |
| 1.4 | ≃26 | $10^{-4}$ | 65 | 300 | 260[4] | 21 | 65–60–59 |
| | | | | | 360[5] | 117 | 27[c] |
| | | | | | | 141 | 22[c] |
| 1.3 | ≃23 | $2 \times 10^{-4}$ | 126 | 460 | | 21 | 60–55–55 |
| | | | | | | 117 | 26[c] |
| | | | | | | 136 | 22[c] |
| **Fe**V | | | | | | $7.4 \times 10^{17}$ | |
| 3.1 | 35 ± 2 | 0 | 42 | — | 140[1] | 20 | 53 |
| 3.2 | 39 | $5 \times 10^{-5}$ | 63 | 400 | 120[2] | 25 | 57 |
| 3.3 | 35 ± 2 | $10^{-4}$ | 88 | 450 | 140[3] | 21 | 58 |
| 3.4 | 27 ± 1 | $10^{-3}$ | 273 | 230 | 90[4] | 21 | 110 |
| 3.5 | 28 ± 1 | $10^{-2}$ | 1370 | 135 | 60[5] | 22 | 230 |
| 3.6 | 38 ± 2 | $3 \times 10^{-2}$ | 2850 | 95 | | 25 | 350 |
| **Fe**V | | | | | | $7.4 \times 10^{17}$ | |
| 4.2 | 112 | 0 | 47 | — | | 37 | 58 |
| 4.3 | 84 ± 1 | $5 \times 10^{-5}$ | 67 | 400 | | 37 | 62 |
| 4.6 | 34 ± 2 | $10^{-4}$ | 78 | 310 | | 20 | 62 |
| 4.1 | 96 ± 1 | $10^{-3}$ | 300 | 250 | | 45 | 105 |
| 4.5 | 101 ± 2 | $10^{-2}$ | 1420 | 140 | | 49 | 260 |
| 4.4 | 98 ± 2 | $3 \times 10^{-2}$ | 3000 | 100 | | 48 | 360 |
| **Fe**Mo | | | | | | $8.0 \times 10^{17}$ | |
| 7.1 | 36.5 | 0 | 63 | — | 160[2] | 30 | 69 |
| 7.2 | 46 | $5 \times 10^{-5}$ | 104 | 800 | 190[4] | 33 | 69 |
| 7.3 | 56 | $10^{-4}$ | 132 | 700 | | 34 | 70 |
| 7.4 | 45 | $4 \times 10^{-4}$ | 278 | 540 | | 33 | 77 |
| 7.5 | 42 | $10^{-3}$ | 470 | 410 | | 32 | 105 |
| 7.6 | 45 | $3 \times 10^{-3}$ | 940 | 290 | | 34 | 180 |
| **Fe**Mo | | | | | | $7.4 \times 10^{17}$ | |
| 8.5 | 49.5 | $10^{-2}$ | 2160 | 210 | | 24 | 210 |
| 8.4 | 49.5 | $3 \times 10^{-2}$ | 4800 | 160 | | 24 | 270 |
| 8.6 | 36.5 | 0 | 80 | — | | 23 | 76 |
| 8.3 | 48 | 0 | 34 | — | | 23 | 55 |
| 9.1 | 41 | 0 | 87 | — | | 23 | 61 |

[a] The first figure of the sample number is the experiment number, the second one refers to the position of the sample on the sample holder. The **Fe**Ti samples underwent five runs (labelled 1a to 1e; see section 6), the first three at ~20 K, the last two at ~120 and 140 K.

[b] Sources: [1] Campbell *et al* (1967); [2] Arajs *et al* (1969), [3] Fert and Campbell (1976), [4] Dorleijn and Miedema (1977); [5] Pierron *et al* (1982). All these determinations have been carried out for solute concentrations between 0.5 and 3 at.%.

[c] The dose for these runs was $16.8 \times 10^{17}$ $e^-/cm^2$.

$$\rho_s^* = [\rho_{4K}(\text{alloy}) - \rho_{4K}(\text{Fe})]/c_s,$$

where $c_s$ is the solute concentration. We have seen in a previous paper (Maury *et al* 1987) that it may depend strongly on the solute concentration. This is the case for the alloy **Fe**Cr; and it is also the case for **Fe**Mo and **Fe**V (see table 1) or **Fe**Mn but not **Fe**Ni (see next paper).

We have shown that this dependence can be well interpreted on the basis of the two-current model developed by Fert and Campbell (1976). It results from the non-additivity (in opposition to Matthiessen's rule) of the resistivity of the solute (which has a spin-up resistivity $\rho_\uparrow$ larger than its spin-down resistivity $\rho_\downarrow$) together with that of the residual impurities (mostly Si atoms for which $\rho_\downarrow$ is larger than $\rho_\uparrow$). The present results corroborate this interpretation since a large effect is observed with those solutes (Mo, V, Mn) for which the ratio $\alpha_s = \rho_\downarrow/\rho_\uparrow$ is smaller than 1 (respectively 0.2, 0.1, 0.1) and not with Ni for which it is larger than 1: $\alpha_{Ni} = 3$ to 7 (Campbell and Fert 1982).

The residual impurities, however, cannot be responsible for differences observed between the 1% and the 3% alloys: the solute specific resistivity is found to be smaller in the 3% alloy than in the 1% alloy, both for **Fe**Mo and **Fe**V (see table 1). Such a large decrease (25 to 30%) of $\rho_s^*$ when the solute concentration $c_s$ goes up from 1% to 3% was not observed in the **Fe**Cr alloys (Maury *et al* 1987). It could result from solute precipitation in Fe + 3% Mo: the solubility limit of Mo in Fe is less than 3 at.% at 700 °C (Moffatt 1980). In the alloy Fe + 3% V, it could come from short-range ordering: the interaction between two solute atoms in first- and second-nearest-neighbour positions is found to be repulsive in this alloy, like in Fe + 3% Cr (Hennion 1983, Mirebeau *et al* 1982, 1984). But the effect of short-range ordering on the alloy resistivity in this concentration range is small (Pierron *et al* 1984) and cannot account for the large variation of $\rho_s^*$ observed between 1 and 3% V. A tentative explanation is given in appendix 2.

### 3.2. *Defect resistivity*

The apparent Frenkel pair specific resistivity is defined as

$$\rho_F^*(\varphi) = \Delta\rho/c_F = [\rho_{4K}(\varphi) - \rho_{4K}(0)]/c_F(\varphi)$$

where $\varphi$ is the electron dose, $c_F$ the radiation-induced Frenkel pair concentration and $\rho_{4K}$ the alloy residual resistivity. Owing to the above-mentioned deviations from Matthiessen's rule, $\rho_F^*$ depends both on the alloy through the solute resistivities $c_s\rho_{s\downarrow}$ and $c_s\rho_{s\uparrow}$ and on the dose through the Frenkel pair resistivities $c_F\rho_{F\downarrow}$ and $c_F\rho_{F\uparrow}$. This dependence is worked out in appendix 1 according to the two-current model.

The resistivity $\rho_F^*$ is always larger than $\rho_F$, the Frenkel pair specific resistivity in pure Fe. It is the larger, the more different the parameters $\alpha_s$ and $\alpha_F$, or $z_s$ and $z_F$, $z$ being defined as $z = (\rho_\downarrow - \rho_\uparrow)/(\rho_\downarrow + \rho_\uparrow)$. Our experimental results show that the measured radiation-induced resistivity $\Delta\rho$, and hence $\rho_F^*$, is much larger for solutes having a negative $z_s$, like V, Mn, Mo, than for solutes with a positive one, like Ni. This indicates a positive value of $z_F$. Now $z_F$ is a mean value (see appendix 1) between the interstitial and the vacancy parameters $z_i$ and $z_v$; $z_v$ is expected to be negative since a vacancy in iron should act like a repulsive potential, i.e. at least qualitatively like a V atom ($z_V \simeq -0.8$), for example. The positive value of $z_F$ is thus likely to result from a large positive value of $z_i$.

This simple model allows one to explain most of the measured resistivity change rates:

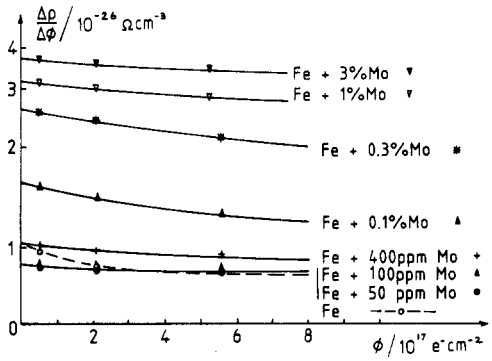


**Figure 1.** Measured resistivity change rate as a function of the electron dose ($E$ = 1.6 MeV) for Fe and **Fe**Mo alloys (runs No 7 and 8).

In our Fe samples, where the main residual impurity is Si (up to ≃20 at. ppm), which has a positive $z$, the initial value of $\rho_F^*$, $(\rho_F^*)_0$, is usually not much larger than $\rho_F$. Moreover, if the residual impurity concentration is low enough, $\rho_F^*$ can approach its saturation value, $\rho_F$, as the irradiation goes on.

In concentrated alloys ($c_s$ = 1 to 3%), $\rho_F^*$ should depend neither on the solute nor on the defect concentration since both the residual impurities and the Frenkel defects are negligible compared to the solute. Yet the measured resistivity change rate is always found to decrease when the dose is increased, even in the most concentrated alloys (see figure 1 for example), but then this decrease is small (3 to 10% when the fluence goes from 2 to 5 × $10^{17}$ $e^-/cm^2$), almost within the experimental uncertainties and part of it may be due to a shift in the beam profile or a slight increase in the temperature as the irradiation proceeds. But again, the 1% and 3% alloys, which should behave similarly, definitely do not. The measured radiation-induced resistivity is found to be larger in the 3% alloys than in the 1% ones; for example $\Delta\rho$ (3% V) = 1.4$\Delta\rho$ (1% V).

If we assume that about the same concentration of defects is produced in both alloys, and since this concentration, which is quite low (≤30 at. ppm with $\rho_F \geq 2.0$ mΩ cm), cannot modify significantly the precipitation or short-range order state of these alloys, it thus follows that $\rho_F^*$, like $\rho_s^*$, is found different in the 1% and 3% alloys. A possible explanation for this difference is given in appendix 2.

In the alloys of intermediate concentrations (1000 to 3000 at. ppm) the initial value of $\rho_F^*$ is intermediate between $\rho_F$ and $\rho_F^*$ in the concentrated alloys; $\rho_F^*$ decreases as $c_F$ increases without the saturation value $\rho_F$ being attainable because $c_F$ cannot grow much larger than $c_s$.

### *3.3. Need for experimental data correction*

It follows from the preceding that since the apparent Frenkel pair specific resistivity $\rho_F^*$ depends on the defect concentration $c_F$, the measured radiation-induced resistivity is not proportional to the defect concentration, and is not a straightforward measure of this concentration. As a consequence the experimental resistivity recovery spectra need to be corrected to reflect the defect recovery. This correction is negligible in the concentrated alloys where $\rho_F^*$ is about constant ($c_F \ll c_s$), but not quite negligible in the metal and the dilute alloys. This is shown by the variations of the fractional resistivity recovery due to Frenkel pair recombination (fraction of the radiation-induced resistivity annealed at 94 K or height of the $I_{D_1}$ recovery peak around 100 K). Correcting the

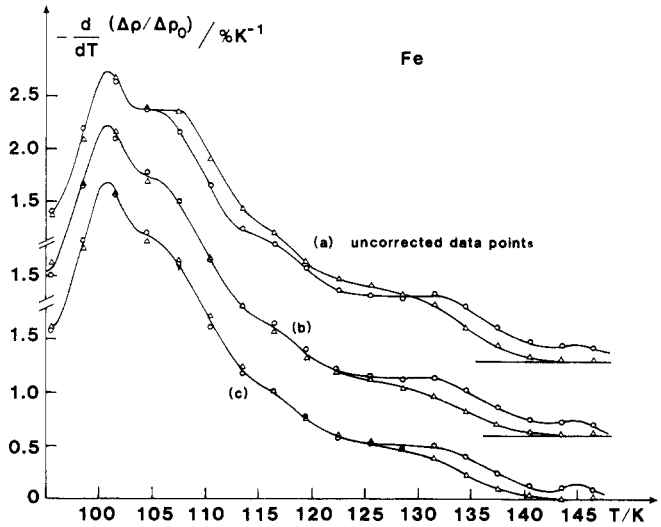


**Figure 2.** Differentiated isochronal recovery spectra of two Fe samples, No 8.3 (○) and 8.6 (△): $T_{irr} \simeq 25$ K; $\Delta t = 300$ s; (*a*) uncorrected data, (*b*) maximal correction, (*c*) medium correction.

experimental recovery spectra according to the two-current model increases the recovery rate at low temperatures and reduces it at the end of the recovery. Such a correction is reliable as long as the recovery is due to Frenkel pair recombination. We will assume as a first approximation that no resistivity change occurs when a migrating split self-interstitial, Fe–Fe, is trapped in the vicinity of a solute atom.

## 4. Stage I and stage II recovery in Fe samples

Nine Fe samples, prepared and annealed successively, either in Grenoble or in Vitry, were irradiated in eight different runs together with the alloy samples, in the present set of experiments. Their residual resistivities varied from 34 to 87 nΩ cm. Their stage I recovery spectra all fall within the two extreme spectra shown in figure 2(*a*), which are those of samples 8.3 prepared in Vitry ($\rho_0 = 34$ nΩ cm) and sample 8.6 prepared in Grenoble ($\rho_0 = 80$ nΩ cm).

A correction based on the two-current model so as to get $c_F/c_{F0}$ from $\Delta\rho/\Delta\rho_0$ makes the two spectra identical within the experimental uncertainties up to 125 K as can be seen from figures 2(*b*) and (*c*). The corrected resistivity data are listed in table 2 with the corresponding values of $\alpha_0$, which is the $\alpha$ parameter of the sample prior to the irradiation. The value of $\alpha_F$ is best taken equal to 10, in agreement with Dunlop's (1980) determination: $\alpha_F = 5$ to 10.

Once corrected, the radiation-induced resistivity, $\Delta\rho_0$, and the fractional extra resistivity retained after close pair recombination, $\Delta\rho(94\text{ K})/\Delta\rho_0$, should not depend on the sample. The fractional extra resistivity retained at the end of stage I, $\Delta\rho(148\text{ K})/\Delta\rho_0$, should increase with increasing purity. These three points are exactly met in (*c*). Correction (*b*) is the largest one compatible with the former requirements, given the experimental uncertainties.

**Table 2.** Uncorrected and corrected stage I recovery data for Fe samples 8.3 and 8.6.

| | | Sample No | $\alpha_0$ | $\Delta\rho_0$ (nΩ cm) | $\Delta\rho(94\text{ K})/\Delta\rho_0$ (%) | $\Delta\rho(148\text{ K})/\Delta\rho_0$ (%) |
|---|---|---|---|---|---|---|
| (*a*) | Uncorrected | 8.3 | — | 55.4 | 70.4 | 12.2 |
| | data | 8.6 | — | 75.7 | 71.8 | 13.1 |
| (*b*) | Maximal | 8.3 | 2.0 | 48.2 | 67.3 | 9.2 |
| | correction | 8.6 | 0.9 | 39.3 | 63.3 | 8.3 |
| (*c*) | Medium | 8.3 | 1.5 | 44.6 | 65.6 | 8.0 |
| | correction | 8.6 | 1.1 | 45.5 | 64.4 | 8.5 |

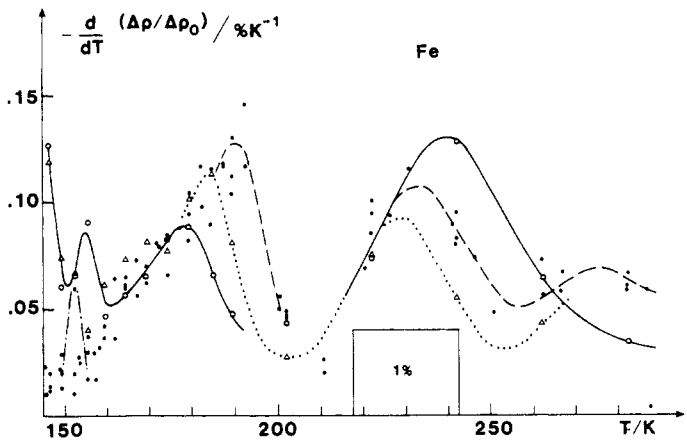


**Figure 3.** Differentiated isochronal recovery spectra of eight Fe samples: No 8.3 (—○—) of minimal residual resistivity ($\rho_0$ = 34 nΩ cm); No 9.1 (····△····) of maximal residual resistivity ($\rho_0$ = 87 nΩ cm); Nos 3.1, 5.2, 6.6, 7.1, 8.6 and 9.1 (---●---) of intermediate residual resistivities; uncorrected data; $\Delta t$ = 300 s.

The stage II and stage III recovery data of all Fe samples are plotted on figure 3. As expected the stage II recovery spectra are much more different from one another than the stage I spectra.

The purest sample (8.3) elaborated in Vitry in a Cu crucible, and annealed together with Fe + 1% Ni and Fe + 3% Ni samples, shows three distinct recovery peaks in stage II. The first one centred around 145 K is related to residual Cu; the second one around 155 K to residual Ni (see the following paper); and the third one, between 160 and 190 K, to residual Si (Maury *et al* 1985) and to poly-interstitials retained by residual impurities. The Fe samples elaborated in Grenoble in a silver crucible do not show any Cu peak, except for one sample annealed in Vitry, nor any Ni peak, except for one sample annealed together with FeNi samples. Their stage II recovery is enhanced between 180 and 200 K, probably because of additional residual impurities.

Stage III, which is attributed to vacancy free migration (Vehanen *et al* 1982), is the larger the purer the sample, as expected. No correction can be validly applied to stage

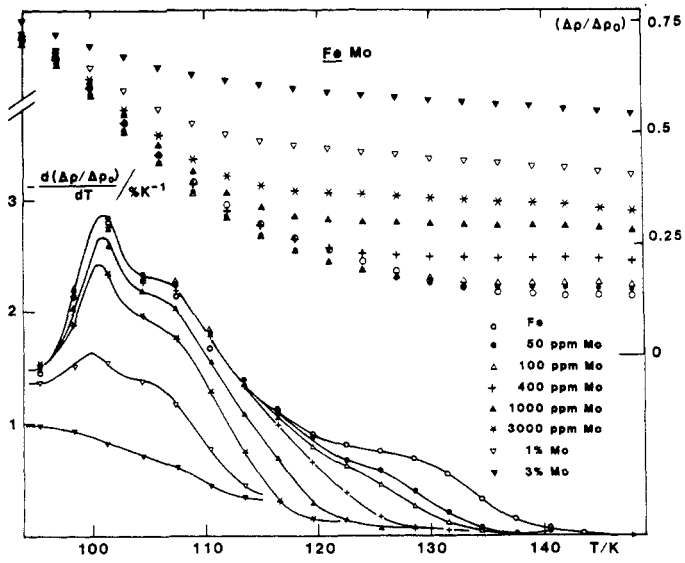


**Figure 4.** Isochronal recovery spectra together with their derivatives of Fe and **Fe**Mo alloys; $T_{irr}$ = 30–35 K; $\Delta t$ = 300 s.

II or III due to the complexity of the defects (mixed and/or poly-interstitials) involved in these stages.

## 5. Interstitial recovery in FeMo alloys

### *5.1. Stage I recovery*

Figure 4 shows the measured resistivity recovery spectra of Fe and **Fe**Mo alloys. Up to 115 K and for a Mo concentration $c_s \leqslant 400$ at.ppm, the spectra are the same, taking into account the variations observed for the various Fe samples. The spectrum of the Fe sample (7.1) is identical to that of sample 8.3 of figure 2. The spectra of Fe + 50 ppm Mo and Fe + 100 ppm Mo are intermediate between those of samples 8.3 and 8.6. For Mo concentrations $c_s \geqslant 400$ at.ppm, correcting the measured spectra for $\rho_F^*$ variations brings in but negligible changes.

The spectra of the dilute **Fe**Mo alloys look similar to those of **Fe**Au alloys (Maury *et al* 1985). Stage $I_E$ between 120 and 140 K is gradually suppressed by increasing concentrations of Mo, indicating that the freely migrating Fe–Fe self-interstitials are getting trapped at the Mo atoms.

The $I_{D_1}$ and $I_{D_2}$ peaks, centred at 101 and 108 K respectively, begin, like the recovery below 94 K, to be reduced when the Mo concentration reaches 0.1 at.%. Figure 4 shows that $I_{D_2}$ as a function of the solute concentration is the same as $I_{D_1}$: both peaks are equally suppressed whatever the solute concentration may be: 0.1, 0.3, 1 and even 3 at.% Mo, which corresponds to a mean distance between the self-interstitial and the nearest solute atom of respectively 5, 3, 2 and 1.5 interatomic distance. This is not consistent with $I_{D_1}$ originating from close pair recombination and $I_{D_2}$ from correlated recombination of free interstitials, as has been assumed previously (Takaki *et al* 1983,

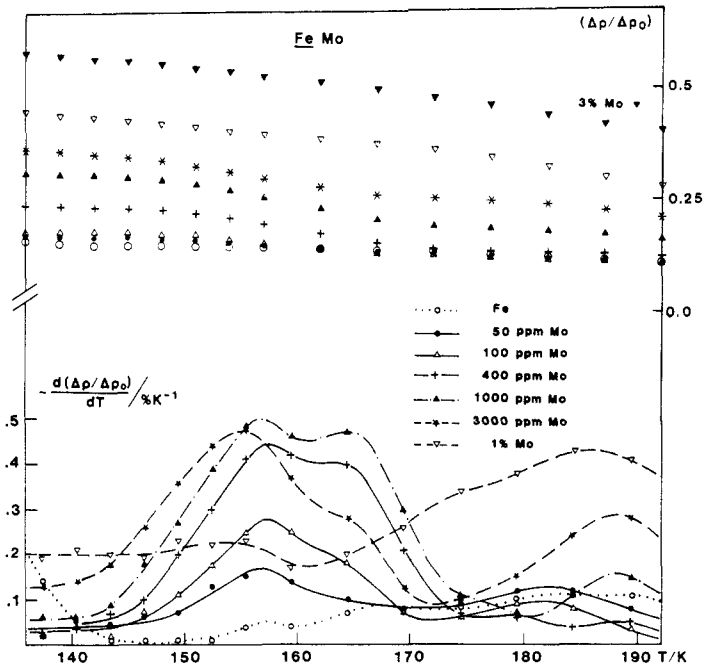


**Figure 5.** Same as figure 4, but at higher temperatures.

Maury *et al* 1985). The present results show that substages $I_{D_1}$ and $I_{D_2}$ must both arise from close pair recombination (and should be better labelled $I_{C_2}$ and $I_{C_3}$). The correlated recombination of free interstitials with vacancies should then take place between 110 and 120 K.

### 5.2. *Stage II recovery*

Figure 5 shows the measured recovery spectra of Fe and **Fe**Mo alloys. If we look at the most dilute alloys (50, 100 and 400 at.ppm), we see a peak centred around 155 K, the height of which increases regularly with increasing Mo concentrations. It does not shift towards low temperatures as the Mo concentration goes up. This indicates (Maury *et al* 1988) that it is a detrapping peak whose position is governed by the binding energy between the solute atom and the self-interstitial. The 155 K peak can thus be attributed to the release of self-interstitials trapped at Mo atoms. It is similar to the peak observed at 160 K in **Fe**Au dilute alloys and also attributed to detrapping of self-interstitials from solute atoms.

In this paper and the following one, we use the term 'trapped interstitial' when the self-interstitial (⟨110⟩ Fe–Fe dumbell) is retained in a neighbour position of a solute atom and 'mixed interstitial' when the solute atom has been pushed out of its lattice site and has replaced one of the two Fe atoms forming the self-interstitial whatever the final configuration may be (⟨110⟩ dumbell or not). That in **Fe**Mo alloys, no mixed interstitial is formed during stage I, is shown by the channelling results of Kiejek and Palmer (1987). It is predictable on the basis of the large positive size effect of Mo in Fe (King 1966) and consistent with the present experiment, where one does not observe any recovery peak

**Table 3.** Percentage of the measured radiation-induced resistivity retained at 172, 192 and 292 K.

| Sample No | $c_s$ | $\Delta\rho(172\text{ K})/\Delta\rho_0$ | $\Delta\rho(192\text{ K})/\Delta\rho_0$ | $\Delta\rho(292\text{ K})/\Delta\rho_0$ |
|---|---|---|---|---|
| 8.6 | 0 | 12.1 | 10.3 | 3.3 |
| 7.1 | 0 | 12.5 | 10.5 | 2.9 |
| 7.2 | $5\times10^{-5}$ | 12.3 | 10.2 | 3.2 |
| 7.3 | $10^{-4}$ | 12.0 | 10.6 | 3.2 |
| 7.4 | $4\times10^{-4}$ | 13.5 | 12.4 | 3.2 |
| 7.5 | $10^{-3}$ | 18.5 | 16.2 | 3.8 |
| 7.6 | $3\times10^{-3}$ | 24.6 | 20.7 | 3.3 |
| 8.5 | $10^{-2}$ | 35.3 | 27.6 | 3.1 |
| 8.4 | $3\times10^{-2}$ | 47.0 | 40.2 | 5.5 |

shifting towards low temperatures as the solute concentration goes up, which would have to be attributed to mixed-interstitial long-range migration. At solute concentrations such as 1000 ppm Mo, high enough to suppress partially the correlated recovery (110–120 K), interstitials, which instead of being annihilated at their correlated vacancy are trapped by solute atoms, are still correlated with their original vacancies. If mixed interstitials were formed and freely migrating around 155 K, this correlation should appear as a shift of the recovery peak towards low temperatures as the solute concentration goes up. In contrast when dissociation takes place (either of trapped or mixed interstitials), and provided the self-interstitial migration energy is small as compared to the trapped (or mixed) interstitial binding energy, it gives rise to a recovery peak whose position is governed mainly by the frequency of the detrapping jump. The subsequent jumps resulting in self-interstitial long range migration are practically instantaneous, so the correlation between interstitials and vacancies is not observable.

A second peak is observed, centred around 165 K, the amplitude of which is maximal for a Mo concentration $c_s = 1000$ at.ppm. This peak can possibly stem from the release of two self-interstitials trapped at the same Mo atom, on opposite sides for example. At low Mo concentration (50 at.ppm) they form in a negligible concentration. The concentration of residual impurities is larger than that of trapped interstitials. At higher Mo concentrations ($c_s \geqslant 3000$ at.ppm), it is the occurrence of multiple trapping (trapping by at least two neighbouring Mo atoms) that hinders their formation. The 165 K peak is lowered as new peaks appear at higher temperature.

The fraction of extra resistivity retained at the beginning of stage III, $\Delta\rho(192\text{ K})/\Delta\rho_0$, increases markedly as the Mo concentration goes up. This increase reflects the incidence of multiple trapping. As shown by table 3, it has been annealed out at the end of stage III: the molybdenum efficiency for interstitial trapping is lost at room temperature. For Mo concentrations larger than 1%, the possible occurrence of precipitates in the $\alpha$-phase impedes a straightforward interpretation of the data. It is not excluded that, like in **Ag**Zn alloys (Régnier and Halbwachs 1980), multiple trapping still plays a role at room temperature in the 3% alloy but not in the 1% one.

## 6. Interstitial recovery in FeTi alloys

Like Mo, Ti is an oversized solute in Fe. Its solubility limit is still lower than that of Mo: 2.3 at.% at 700 °C (Moffatt 1980). The apparent Ti specific resistivity (see table 1) was

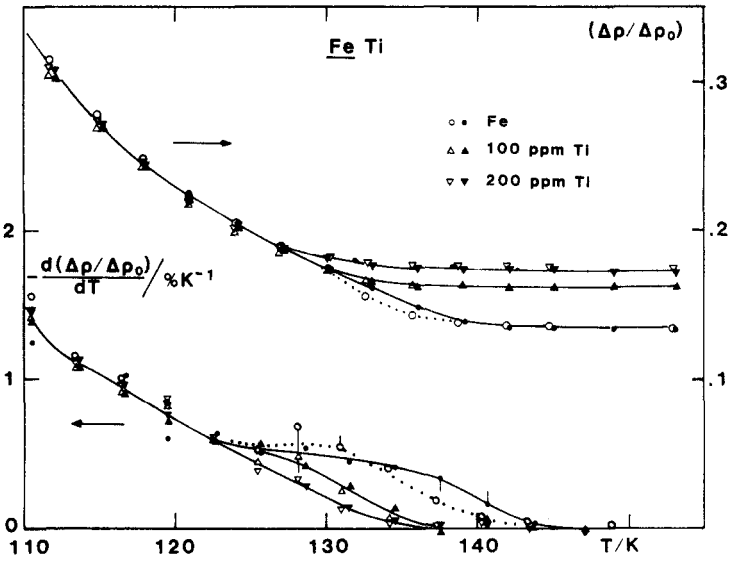


**Figure 6.** Isochronal recovery spectra together with their derivatives, of Fe and **Fe**Ti alloys; $T_{irr} \simeq 20$ K; $\Delta t = 300$ s; open symbols, run No 1b; full symbols, run No 1c.

found to be larger in the alloy Fe +200 ppm Ti than in Fe +100 ppm Ti, indicating that either some Ti has been lost in the 100 ppm alloy or that some extra pollution has occurred in the 200 ppm alloy. Ti oxidises easily (Bénard *et al* 1984) and the oxides TiO and $TiO_2$ are not volatile like SiO, $VO_2$ or $Al_2O$.

The **Fe**Ti experiment was the first performed of all the experiments reported here. Because of the low Ti solubility, no concentrated alloys (in the per cent range) were prepared and irradiated. The sample chamber was the same as used previously for the **Fe**Cr experiments. It had a small thermal inertia, which allowed rapid changes from measuring to annealing temperature but resulted in a poorer stability of the annealing temperature, and thus poorer reproducibility of the recovery spectra from one run to the other.

### *6.1. Stage I recovery*

Five irradiation runs were performed successively: runs No 1a, 1b, 1c at 20 K to a fluence of $6.3 \times 10^{17}$ $e^-/cm^2$ and runs No 1d and 1e, at 120 and 140 K respectively, to a fluence of $16.8 \times 10^{17}$ $e^-/cm^2$. Between each run, the samples were kept for several days at room temperature. The extra resistivity left in the samples varied from 0.3 to 3.5% of their residual resistivity or from 1.1 to 2.5% of the radiation-induced resistivity at 20 K, depending on the sample and on the run.

Figure 6 shows the measured stage $I_E$ recovery spectra after run No 1b (open symbols) and run No 1c (full symbols). The two Fe spectra do not coincide at the end of stage $I_E$; this may stem from the modification of the residual impurities distribution through radiation-induced solute diffusion after run No 1b. The **Fe**Ti spectra are not changed significantly.

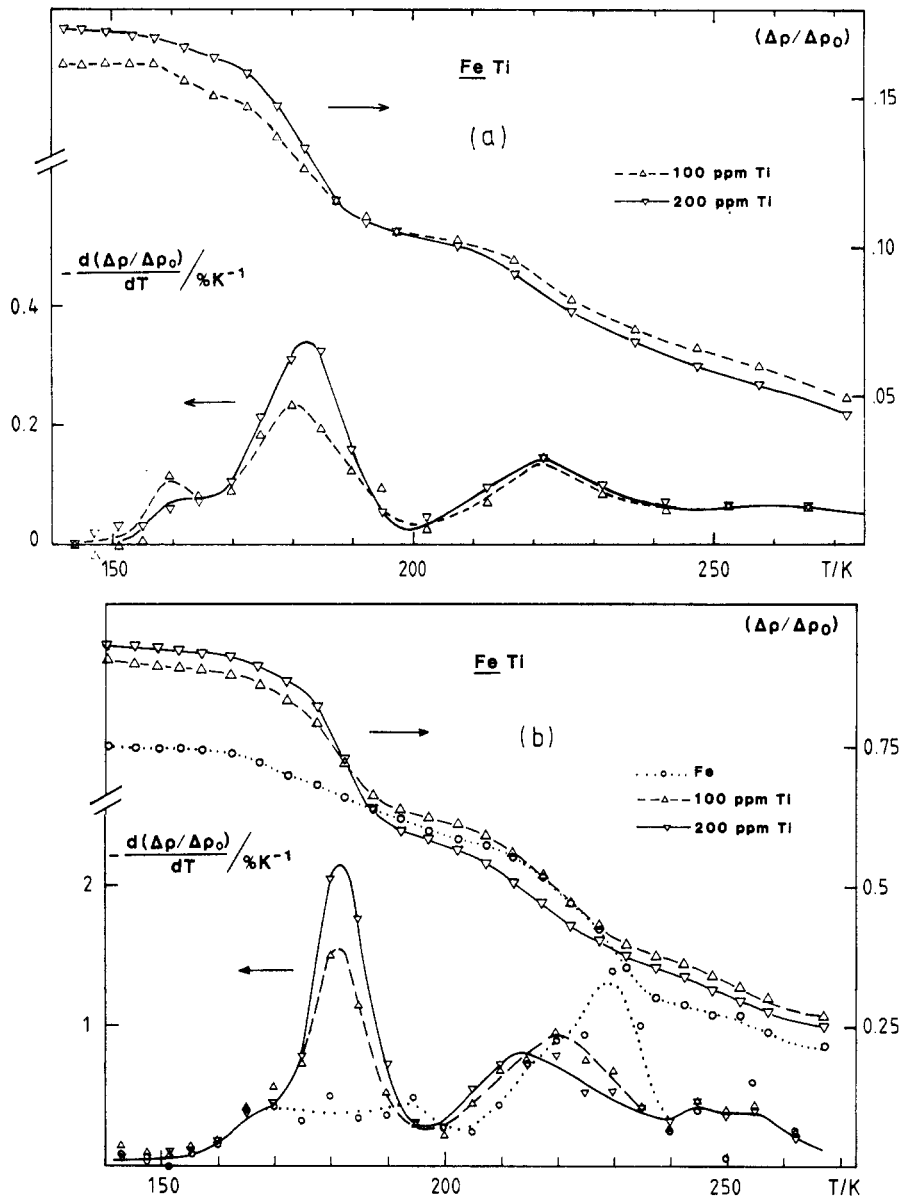


**Figure 7.** Isochronal recovery spectra together with their derivatives, of Fe and FeTi alloys; (*a*) run No 1c; $T_{irr} = 20$ K, (*b*) run No 1d; $T_{irr} \simeq 120$ K; $\Delta t = 300$ s.

Stage $I_E$ is suppressed by 100 and 200 ppm Ti as it is by 50 and 100 ppm Mo, indicating that, like the Mo atoms, the Ti atoms do trap the migrating self-interstitials.

### *6.2. Stage II recovery*

Figure 7 shows the stage II (150–200 K) and stage III (200–250 K) recovery spectra measured after run 1c ($T_{irr} = 20$ K, $\varphi = 6.3 \times 10^{17}$ e$^-$/cm$^2$) and 1d ($T_{irr} = 120$ K, $\varphi =$

$17 \times 10^{17}$ e$^-$/cm$^2$). Quite similar spectra were recorded after run 1e ($T_{irr}$ = 140 K, same dose) except that stage II was enhanced, in Fe by a factor 2, and in Fe + 100 ppm Ti by a factor 1.5.

In stage II, one peak, at 180 K, is related to the presence of Ti. Its position does not depend appreciably on the solute content nor on the dose: 181 ± 1 K after runs 1c, 1d and 1e. Its amplitude increases with increasing concentrations of Ti; it is about the same (if measured after run 1c, or if normalised to the 20 K radiation-induced resistivity after runs 1d, 1e) as that of the 155 K peak of **Fe**Mo. The most straightforward interpretation of the present results is to ascribe this peak to the detrapping of single Fe interstitials trapped at substitutional Ti atoms. That no mixed interstitials are formed cannot indeed be inferred from the present experiment: the 180 K peak could as well be attributed to the dissociation of Fe–Ti mixed interstitials. The existence of Fe–Ti mixed interstitials has been assumed by Walz *et al* (1982) to interpret magnetic relaxation spectra. It seems to us unlikely on the basis of size effect considerations but cannot be excluded. What the present experiment shows is that the stage II recovery is much different in **Fe**Ti than in **Fe**Ni (Maury *et al* 1986) or in **Fe**Si (Maury *et al* 1985). In **Fe**Ni a peak $II_{Ni}$ is observed, which shifts from 145 K for 100 ppm Ni to 140 K for 400 ppm Ni. Its amplitude increases markedly with the solute concentration. This peak is attributed to the free migration of Fe–Ni mixed interstitials not retrapped by Ni atoms. In **Fe**Si a peak $II_{Si}$ is observed, which shifts from 180 K for 50 ppm Si to 175 K for 400 ppm Si. Its amplitude does not depend much on the solute concentration. This peak is attributed to the free migration of Fe–Si mixed interstitials retrapped by Si atoms. The 180 K peak in the **Fe**Ti alloys behaves with the solute concentration quite differently from peaks $II_{Ni}$ or $II_{Si}$. On the other hand its behaviour is comparable to that of the 155 K peak of **Fe**Mo or the 160 K peak of **Fe**Au. We then attribute it to the release of self-interstitials from Ti traps or, if mixed interstitials were formed, to their dissociation.

Stage III is suppressed by the addition of Ti, which is consistent with the positron annihilation results of Corbel (1986): Ti impedes the clustering of vacancies up to 350 K.

## 7. Interstitial recovery in FeV alloys

Vanadium is highly soluble in iron (its solubility limit is ~30%). Its size effect is still positive, but smaller than those of Au, Mo or Ti.

We irradiated two sets of **Fe**V samples. The first ones were chemically thinned from ~100 to 30 $\mu$m and then annealed. The second ones (except for sample 4.6) were just cleansed and then annealed. The residual resistivity of the Fe sample was only slightly higher in the latter case (47 instead of 42 n$\Omega$ cm). Its stage II recovery however was quite different, being much enhanced between 170 and 200 K, which indicates that some surface pollution has not been entirely removed in that case.

### *7.1. Stage I recovery*

Figure 8 shows the measured recovery spectra of the two sets of samples. Both sets were irradiated with the same electron flux, resulting in a higher temperature for the thick samples (40–50 K) than for the thin ones (20–25 K).

The points of figure 8 are raw data. The first run data (figure 8(*a*)) can be corrected

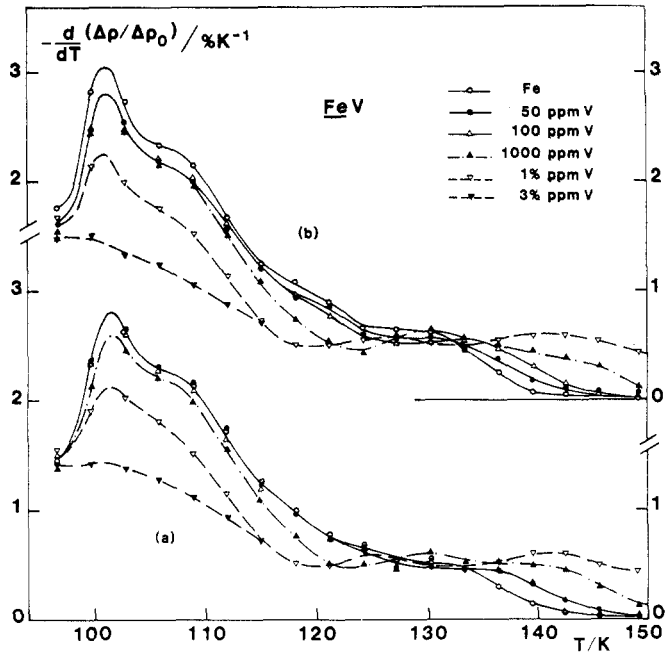


**Figure 8.** Differentiated isochronal recovery spectra of Fe and **Fe**V alloys: (*a*) run No 3, thin samples, $T_{irr}$ = 20 K; (*b*) run No 4, thick samples, $T_{irr}$ = 44–55 K; $\Delta t$ = 300 s.

for the variations of $\rho_F^*$ with the values of $\alpha_0$ (mean $\alpha$ prior to the irradiation) listed below and with $\alpha_F = 10$:

| Sample | Fe | Fe + 50 ppm V | Fe + 100 ppm V | Fe + 1000 ppm V |
|---|---|---|---|---|
| $\alpha_0$ | 1.7–2.5 | 1.7–2.5 | 1.7–2.5 | 0.9–1.1 |

The $\alpha_0$ range is determined so as to yield a constant radiation-induced resistivity, $\Delta\rho_F = 45 \pm 5$ nΩ cm, and a constant fractional recovery up to 94 K, $\Delta\rho(94\text{ K})/\Delta\rho_0 =$ 64 to 67%. This $\rho_F^*$ correction (not shown on figure 8) does not modify appreciably the relative disposition of the curves; it is negligible for 1 and 3%. As concerns the second run data (figure 8(*b*)) no correction can reasonably be done since the variations of the irradiating temperature, due to thickness differences from one sample to another, may be responsible for some part of the $\Delta\rho_F$ or $\Delta\rho(94\text{ K})/\Delta\rho_0$ variations. Yet it appears that the $\rho_F^*$ correction for the Fe sample (4.2) has to be unusually small as shown by the figures in table 4. This again indicates that some superficial pollution was not removed in that case; it shows furthermore that these additional impurities must have (like Si, Al, Ga, . . .) an $\alpha$ parameter larger than the usual $\alpha_0$ of our Fe samples.

If we now compare the recovery data for the two runs, we see that the two 100 ppm spectra are identical within the experimental uncertainties (no thick sample was available for that concentration); so are the 1000 ppm and 1% spectra, which are not sensitive to the residual impurities. The Fe and Fe + 50 ppm V spectra are the only ones that differ from one run to the other: (i) in the $I_D$ region because the $\rho_F^*$ correction is larger for the

**Table 4.** The $\rho_F^*$ corrections for Fe.

| | Sample 4.2 uncorrected (%) | All other Fe samples | |
|---|---|---|---|
| | | uncorrected (%) | after $\rho_F^*$ correction (%) |
| $\Delta\rho(94\text{ K})/\Delta\rho_0$ | $\leqslant 68.5$ | 69.5—71.8 | 65–66 |
| $\Delta\rho(142\text{ K})/\Delta\rho_0$ | $\leqslant 9$ | 12.1–14.0 | 8.5–10 |

thin samples and (ii) in the $I_E$ region because the thin samples are purer than the thick ones.

One striking feature that shows up from figure 8 is an apparent enhancement of the recovery at the end of stage $I_E$ as the V content increases. In fact the corrected fraction of extra resistivity retained at 151 K is constant for the most dilute alloys (up to 100 ppm), $\Delta\rho(151\text{ K})/\Delta\rho_0 = (10 \pm 1)\%$, showing that the enhancement of the recovery at the end of stage $I_E$ cancels a previous reduction. This is more clearly visible for the 1000 ppm sample. In that sample the cancellation is not complete so that $\Delta\rho(151\text{ K})/\Delta\rho_0$ is still higher in the alloy (13 to 14%) than in the metal (10%).

This suggests that the defects that recover at the end of stage $I_E$ are those which have not been annealed out in stage $I_D$ or at the beginning of stage $I_E$, i.e. the interstitials that have been trapped during their migration. The reduction of substages $I_{D_1}$ and $I_{D_2}$ (around 101 and 108 K) in the most concentrated alloys, which is comparable with (although of slightly less amplitude than) that observed in **Fe**Mo alloys (figure 4), confirms that, like the Mo atoms, the V atoms do trap the migrating Fe interstitials. Moreover, like in the **Fe**Mo alloys, the recovery below 94 K also begins to shrink as the solute concentration reaches 1000 ppm.

The most straightforward interpretation of the present stage I data is thus that Fe self-interstitials are trapped at V atoms but with a small binding energy, so that they are easily released and their recovery is merely shifted towards high temperatures by ~10 K. As the vanadium concentration goes up to 0.1 and 1 at.%, the migrating self-interstitials get trapped closer to their vacancies, so that the initial correlation between interstitials and vacancies can be, at least partially, preserved and gives rise to the structure observed between 120 and 140 K. This structure is observable only because the binding energy is small compared to the migration energy. As the vanadium concentration goes up, the correlated recovery of the trapped interstitials is shifted towards low temperatures (because of increased correlation between vacancies and trapped interstitials) while their uncorrelated recovery is shifted towards high temperatures (because of the lower concentration of interstitials which escape the correlated recovery and lower interstitial effective diffusion coefficient).

### *7.2. Stage II recovery*

As said before, the fractional extra resistivity retained at the end of stage II is the same in the most dilute alloys (50 and 100 ppm V) as in the metal. It starts increasing in the 1000 ppm alloy. At the same time a new peak appears in the stage II range, centred

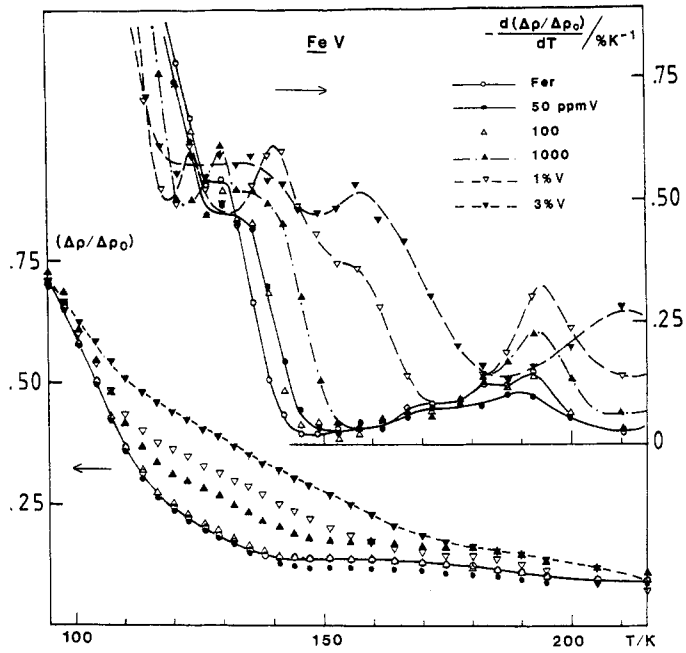


**Figure 9.** Same as figure 8(*a*), but over a wider temperature range.

around 190 K (figure 9). This peak, which is suppressed in the 3% alloy (whilst already significant in the 1000 ppm alloy), more likely comes from the evaporation of small poly-interstitials nucleated on V atoms than from multiple trapping. If we compare the **Fe**Mo and **Fe**V alloys, we see that the incidence of multiple trapping is much reduced in the **Fe**V alloys as compared to the **Fe**Mo alloys. Multiple trapping appears to play an important role only in the Fe + 3% V alloy, where it flattens the stage I recovery between 120 and 140 K and enhances the stage II recovery between 150 and 180 K. This difference can be related to the high solubility of V in Fe; strong repulsive interactions between first- and second-nearest-neighbouring vanadium atoms have been reported (Mirebeau *et al* 1982), which prevents the V atoms from getting close neighbours, while on the contrary in **Fe**Mo, the phase $Fe_3Mo_2$ tends to precipitate as soon as the Mo concentration reaches a few per cent.

Let us note finally that, like in **Fe**Mo, and here up to the most concentrated alloy (Fe + 3% V), the fractional resistivity retained at 292 K is the same in the alloy and in the metal. This shows that the vanadium efficiency for interstitial trapping is lost at room temperature, even in the most concentrated alloys (a few per cent of vanadium).

The present interpretation where the self-interstitials are solely slowed down by the presence of V is quite consistent with the magnetic relaxation measurements of Blythe *et al* (1982). The 110 K relaxation peak attributed to Fe self-interstitials is reduced in Fe + 0.5% V as compared to Fe. At the same time a new peak appears centred around 120 K, which is annealed out at 150 K. The onset of the 83 K relaxation peak related to residual impurities (mixed interstitials Fe–Si for example) is slightly delayed. Finally the 125 K relaxation peak, attributed to poly-interstitials, stable up to stage III, is

**Table 5.**

| Solute | V | Mo | Au | Ti |
|---|---|---|---|---|
| $T_{II}$ (K) | 140 | 155 | 160 | 180 |
| Volume size factor of the solute in Fe (%) | +10 | +27.5 | +44 | +14.5 |
| Volume size factor of Fe in the solute (%) | −19 | | −20 | −54 |
| Pauling metallic radius (Å) | 1.34 | 1.39 | 1.44 | 1.47 |
| Goldschmidt atomic radius (Å) | 1.36 | 1.40 | 1.44 | 1.47 |
| Vegard's law factor (%) | −6.3 | −3.6 | +0.1 | −23.7 |

suppressed, which can be understood as resulting from the formation of small aggregates nucleated on the V atoms rather than larger clusters nucleated on the residual impurities.

## 8. Conclusions

The present set of experiments shows that:

8.1. *Iron self-interstitials* created by electron irradiation and migrating on subsequent annealing throughout stage I do get trapped at all the oversized solute atoms investigated up to now: Te (Swanson *et al* 1980), Au (Swanson *et al* 1980, Maury *et al* 1985), Mo (Kiejek and Palmer 1987, present work), Ti and V (present work).

8.2. *For all these solutes*, the measurements show no sign of the existence of a mixed interstitial. If we look at the magnetic properties of Mo (or V) in Fe (solute moment and host moment perturbation), we note that they are comparable to those of Cr (Stearns 1976). The different trapping properties of these solutes are then to be related to their different sizes: the volume size factor of Cr in Fe is small (+4%) and makes the formation of a mixed interstitial Fe–Cr possible, while the large size of Mo atoms enables the trapping of Fe–Fe self-interstitials to occur on neighbouring sites.

8.3. *The trapped interstitials* are released in stage II at a temperature $T_{II}$ depending on the solute and given in table 5, together with the volume size factor (King 1966) and the atomic radius of the solute. (The Pauling and Goldschmidt radii of Fe equal 1.26 and 1.28 Å respectively.)

If we now look at the strengths of the trapping as a function of the size effect of the solute in Fe (table 5), we see that Ti behaves differently from V, Mo or Au. This is not so if we consider the other parameters like the size effect of Fe in the solute or the solute atomic radius. The strong binding between the Fe self-interstitials and the Ti substitutional atoms can be related to the strong modification of the electronic environment of the Ti atoms when in solid solution in iron, indicated by the large Vegard's law factor of Ti in Fe. The trapping configuration might be different with a Ti atom than with a V, Mo or Au atom. For example, the split interstitial could be trapped in first-neighbour position of a Ti atom, but in second-neighbour position of a V, Mo or Au atom.

8.4. *The most straightforward interpretation of the present data* (although in the case of FeTi, only a limited solute concentration range was available) is that, whatever may be the case (trapped or mixed interstitial), self-interstitials are released in stage II via a

dissociation mechanism. Thus none of these solutes should be able to undergo long-range diffusion in iron through an interstitialcy mechanism. They influence the low-temperature radiation-induced defect annealing only by providing nucleation centres for small interstitial clusters and traps for vacancies.

**Acknowledgments**

The authors wish to thank C de Novion for critical reading of the manuscript, and I A Campbell and A Fert for a judicious comment on the spin-mixing resistivity in Fe.

## Appendix 1. Residual resistivity of Frenkel defects in iron-based alloys according to the two-current model

The two-current model developed by Fert and Campbell (1976) is based on the following assumptions:

(i) The spin $\downarrow$ and spin $\uparrow$ electrons carry current in parallel.

(ii) At low temperatures and as a first approximation, spin-flip scattering is negligible; there is no spin mixing and the two currents are independent.

(iii) Matthiessen's rule is obeyed for each current; each solute has a residual resistivity $\rho_{s\downarrow}$ for the spin $\downarrow$ current and $\rho_{s\uparrow}$ for the spin $\uparrow$ current. Here (and except for the Frenkel pairs) we define $\rho_s$ as the residual resistivity of the solute instead of its specific resistivity, to get rid of the concentration multiplying factor and shorten the equations.

Alternative sets of parameters can be used in place of $\rho_\downarrow$ and $\rho_\uparrow$; the most commonly used are $\rho$ and $\alpha$, defined as follows:

$$\alpha = \rho_\downarrow / \rho_\uparrow$$

and

$$\rho^{-1} = \rho_\downarrow^{-1} + \rho_\uparrow^{-1}$$

where $\rho$ is the solute residual resistivity in the ideal metal.

We will use in the following the two more practical parameters:

$$z = (\rho_\downarrow - \rho_\uparrow)/(\rho_\downarrow + \rho_\uparrow) = (\alpha - 1)/(\alpha + 1)$$

and

$$R = \rho_\downarrow + \rho_\uparrow = \rho(\alpha + 1)^2/\alpha = 4\rho/(1 - z^2).$$

Matthiessen's rule is obeyed for each current: $R$ is then an additive parameter. In an alloy containing $n$ different residual impurities, solutes or defects

$$R = \sum_i R_i.$$

The $z$ parameter is a monotonic function of $\alpha$ which varies from $z = -1$ (when $\rho_\downarrow \ll \rho_\uparrow$ or $\alpha \to 0$) to $z = +1$ (when $\rho_\downarrow \gg \rho_\uparrow$ or $\alpha \to \infty$).

One can show easily that the $z$ parameter of an alloy containing $n$ different residual impurities, solutes or defects is a mean value between the $z$ parameters of each solute

or defect. Let us consider a ternary alloy containing only two solutes 1 and 2; its residual resistivity for the $\downarrow$ and $\uparrow$ currents is

$$\rho_{\downarrow} = \rho_{\downarrow 1} + \rho_{\downarrow 2} \qquad \text{and} \qquad \rho_{\uparrow} = \rho_{\uparrow 1} + \rho_{\uparrow 2}$$

Then

$$R = \rho_{\downarrow} + \rho_{\uparrow} = R_1 + R_2$$

and

$$z = (\rho_{\downarrow} - \rho_{\uparrow})/(\rho_{\downarrow} + \rho_{\uparrow}) = (R_1 z_1 + R_2 z_2)/(R_1 + R_2).$$

The $z$ (or $\alpha$) value of this alloy is a mean value between $z_1$ and $z_2$ (or $\alpha_1$ and $\alpha_2$). If the alloy contains $n$ solutes, its $z$ parameter is

$$z = z_0 = \sum_i R_i z_i \Big/ \sum_i R_i,$$

an average of all $z_i$. If this alloy is now irradiated up to a Frenkel pair concentration $c_F$, its $z$ (or $\alpha$) parameter will gradually move as the irradiation proceeds from $z_0\,(\alpha_0)$ towards $z_F\,(\alpha_F)$, where $z_F$ is the Frenkel pair $z$ parameter. Its residual resistivity will be given by

$$\rho = (1 - z^2)R/4 = [1 - (R_0 z_0 + R_F z_F)^2/(R_0 + R_F)^2](R_0 + R_F)/4$$

the measured radiation-induced resistivity by

$$\Delta\rho = \rho - \rho_0 = \{1 + [R_0/(R_0 + R_F)][(z_0 - z_F)^2/(1 - z_F^2)]\}R_F(1 - z_F^2)/4$$

and the apparent Frenkel pair specific resistivity by

$$\begin{aligned}\rho_F^*/\rho_F &= 1 + [R_0/(R_0 + R_F)][(z_0 - z_F)^2/(1 - z_F^2)] \\ &= 1 + (z_0 - z_F)^2/[1 - z_F^2 + (1 - z_0^2)\rho_F c_F/\rho_0]. \qquad \text{(A1.1)}\end{aligned}$$

$\rho_F^*$ is always larger than $\rho_F$. In concentrated alloys where the residual impurities are negligible as compared to the solute ($z_0 \simeq z_s$), and provided the model is valid (no spin mixing), the initial apparent Frenkel pair specific resistivity, $(\rho_F^*)_0$, is given by

$$(\rho_F^*)_0 = \rho_F[1 + (z_s - z_F)^2/(1 - z_F^2)].$$

The quantity $\{[(\rho_F^*)_0/\rho_F] - 1\}^{1/2}$ measured for different solutes should then be found proportional to $|z_s - z_F|$.

## Appendix 2. Residual resistivity of solute and defects in FeV alloys, taking into account the spin-mixing collisions

According to the hypotheses of appendix 1 (two independent currents, Matthiessen's rule obeyed for each current), the specific resistivity of a solute in a binary alloy where the residual impurities are negligible as compared to the solute should not depend on the solute concentration, i.e. the alloy residual resistivity $\rho_0$ should be proportional to the solute concentration. This is not the case of our FeV alloys, for example, where $\rho_{4K}(\text{Fe} + 3\%\ \text{V})/[3\rho_{4K}(\text{Fe} + 1\%\ \text{V})] = 0.7$.

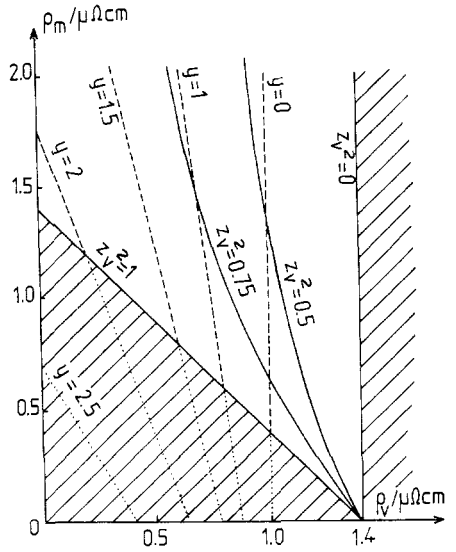


**Figure 10.** Calculated spin-mixing resistivity $\rho_m$, in the alloy Fe + 1% V, as a function of $\rho_V$ (resistivity of 1% V in pure Fe) for various values of the parameters $z_V$ and $y = \rho_{\downarrow\uparrow}$ (3% V)/$\rho_{\downarrow\uparrow}$(1% V).

Moreover, according to equation (A1.1), $\rho_F^*$ should not depend on $c_F$ nor on $\rho_0$ provided $\rho_F c_F \ll \rho_0$, which is always the case with our most concentrated alloys. This second point also is not obeyed. For example, $\rho_F^*$(Fe + 3% V)/$\rho_F^*$(Fe + 1% V) = 1.4.

Let us show that both effects can be explained by taking into account spin-mixing scatterings, not negligible in these $\alpha$-iron-based alloys even at 4 K.

If $\rho_{\downarrow\uparrow}$ is the resistivity arising from these scatterings, the alloy resistivity is given, quite generally, according to Fert and Campbell (1976), by

$$\rho = [\rho_\downarrow \rho_\uparrow + \rho_{\downarrow\uparrow}(\rho_\downarrow + \rho_\uparrow)]/[\rho_\downarrow + \rho_\uparrow + 4\rho_{\downarrow\uparrow}].$$

Values of the parameters $\rho_\downarrow$, $\rho_\uparrow$ and $\rho_{\downarrow\uparrow}$ can be determined to fit the measured values: $\rho_{4K}$(Fe + 1% V) = 1.4 $\mu\Omega$ cm and $\rho_{4K}$(Fe + 3% V) = 3.0 $\mu\Omega$ cm.

Let us define the following parameters:

$$\rho_V = \rho(1\%\ \mathrm{V}) = \rho_\downarrow(1\%\ \mathrm{V})\rho_\uparrow(1\%\ \mathrm{V})/[\rho_\downarrow(1\%\ \mathrm{V}) + \rho_\uparrow(1\%\ \mathrm{V})]$$

$$z_V = (\rho_\downarrow - \rho_\uparrow)/(\rho_\downarrow + \rho_\uparrow)$$

$$\rho_m = \rho_{\downarrow\uparrow}(1\%\ \mathrm{V})$$

and

$$y = \rho_{\downarrow\uparrow}(3\%\ \mathrm{V})/\rho_m.$$

The above equation can then be written for the two alloys:

$$\rho(\mathrm{Fe} + 1\%\ \mathrm{V}) = (\rho_V + \rho_m)/[1 - z_V^2)\rho_m/\rho_V] = 1.4\ \mu\Omega\ \mathrm{cm} \qquad (A2.1)$$

and

$$\rho(\mathrm{Fe} + 3\%\ \mathrm{V}) = (3\rho_V + y\rho_m)/[1 + (1 - z_V^2)y\rho_m/3\rho_V] = 3.0\ \mu\Omega\ \mathrm{cm}. \qquad (A2.2)$$

The full curves of figure 10 show $\rho_m$ as a function of $\rho_V$, deduced from equation (A2.1), for various values of $z_V^2$ between 0 and 1. The broken lines show $\rho_m$ as a function

**Table 6.** Radiation-induced resistivity $\Delta\rho_0$ (n$\Omega$ cm).

| Alloy | Measured values | Calculated values |
|---|---|---|
| Fe + 1% V | 230–255 | 240–315 |
| Fe + 3% V | 350–360 | 320–380 |

of $\rho_V$, deduced from equations (A2.1) and (A2.2), for various values of $y$ between 1 and 3. One sees that assuming $z_V^2 \leqslant 0.75$, which corresponds to $\alpha_V \geqslant 0.07$ and seems reasonable since the values of $\alpha_V$ in the literature lie between 0.10 and 0.13, leads to

$$y \leqslant 1 \qquad \text{i.e.} \qquad \rho_{\downarrow\uparrow}(3\%\ \text{V}) \leqslant \rho_{\downarrow\uparrow}(1\%\ \text{V}).$$

Let us suppose that the spin-mixing scatterings are the same in the two alloys. With $\alpha_V = 0.07$ to 0.10 ($z_V^2 = 0.67$ to 0.76), one gets

$$\rho_V = 0.6 \text{ to } 0.7\ \mu\Omega\text{ cm} \qquad \text{and} \qquad \rho_m = 1.3 \text{ to } 2.0\ \mu\Omega\text{ cm}.$$

This spin-mixing resistivity is not negligible at all. According to Fert and Campbell (see their review article, Campbell and Fert (1982)), spin mixing is imputable to the electron–magnon collisions; it can indeed be very small when there is no impurity or phonon scattering, and become important when impurity scattering makes the spin $\downarrow$ and spin $\uparrow$ mean free paths different, which is the case of the two alloys Fe + 1% V and Fe + 3% V.

The value deduced for $\rho_m$ can be compared to that estimated by Jaoul and Campbell (1975) in nickel: $\simeq 0.3\ \mu\Omega$ cm. Since the internal induction is much larger in Fe than in Ni, this value does not look unreasonable.

The deduced vanadium specific resistivity when spin mixing is negligible (that is at low temperature, for low concentrations of vanadium in pure iron) is $\rho_s = 60$ to $70\ \mu\Omega$ cm. It is close to the value, 62 $\mu\Omega$ cm, extrapolated by Pierron *et al* (1982) from ternary **Fe**SbV alloys.

An alternative interpretation of our resistivity measurements, as pointed out by Jaoul and Campbell (1975), could be the existence in the alloys of a more or less constant concentration of 'unwanted' impurities with a $z$ parameter $z_u \simeq 0$. For example, if one assumes $0.07 \leqslant \alpha_V \leqslant 0.13$ and $\alpha_u \simeq 1$, the residual resistivity of the two alloys can be well reproduced with $\rho_V = 0.8\ \mu\Omega$ cm and $\rho_u = 0.35$ to $0.40\ \mu\Omega$ cm. These values of $\rho_u$ are larger than the residual resistivity of the Fe + 1000 ppm V alloy (275 to 300 n$\Omega$ cm) and are hardly understandable, even if one assumes that some hydrogen or oxygen pollution may be facilitated by the presence of vanadium.

Finally, let us turn to the radiation-induced resistivity; it can be calculated with the values of $\rho_F c_F$ (45 n$\Omega$ cm) and $\alpha_F$ (10) used to correct the dilute alloy spectra. The calculated $\Delta\rho_0$ are found to agree quite well with the experimental ones as shown by table 6.

## References

Arajs S, Schwerer F C and Fisher R M 1969 *Phys. Status Solidi* **33** 731
Bénard J, Michel A, Philibert J and Talbot J 1984 *Métallurgie Générale* (Paris: Masson) p 472
Blythe H J, Dworschak F, Richardson I M and Walz F 1982 *Phys. Status Solidi* a **69** K97

Campbell I A and Fert A 1982 *Ferromagnetic Materials* ed E P Wohlfahrt (Amsterdam: North-Holland) p 768
Campbell I A, Fert A and Pomeroy A R 1967 *Phil. Mag.* **15** 977
Corbel C 1986 *Rapport* CEA-R-5334
Dederichs P H, Lehmann C, Schober H R, Scholz A and Zeller R 1978 *J. Nucl. Mater.* **69–70** 176
Dorleijn J W F and Miedema A R 1977 *J. Phys. F: Met. Phys.* **7** L23
Dunlop A 1980 *Rapport* CEA-R-5053
Fert A and Campbell I A 1976 *J. Phys. F: Met. Phys.* **6** 849
Hennion M 1983 *J. Phys. F: Met. Phys.* **13** 2351
Jaoul O and Campbell I A 1975 *J. Phys. F: Met. Phys.* **5** L69
Kiejek M M and Palmer D W 1987 *Mater. Sci. Forum* **15–18** 703
King H W 1966 *J. Mater. Sci.* **1** 79
Lucasson P, Maury F and Lucasson A 1985 *Radiat. Eff. Lett.* **85** 219
Maury F, Lucasson A, Lucasson P and Dimitrov C 1988 *J. Phys. F: Met. Phys.* **18** 657
Maury F, Lucasson A, Lucasson P, Loreaux Y and Moser P 1986 *J. Phys. F: Met. Phys.* **16** 523
Maury F, Lucasson A, Lucasson P, Moser P and Loreaux Y 1985 *J. Phys. F: Met. Phys.* **15** 1465
Maury F, Lucasson P, Lucasson A, Faudot F and Bigot J 1987 *J. Phys. F: Met. Phys.* **17** 1143
Mirebeau I, Cadeville M C, Parette G and Campbell I A 1982 *J. Phys. F: Met. Phys.* **12** 25
Mirebeau I, Hennion M and Parette G 1984 *Phys. Rev. Lett.* **53** 687
Moffatt W G 1980 *The Handbook of Binary Phase Diagrams* (Berlin: Genium) vol III
Pierron V, Cadeville M C and Gerrer X 1982 *J. Phys. F: Met. Phys.* **12** 969
Pierron-Bohnes V, Mirebeau I, Balanzat E and Cadeville M C 1984 *J. Phys. F: Met. Phys.* **14** 197
Régnier P and Halbwachs M 1980 *Proc. Int. Conf. on Electron Microscopy* vol 4, p 204
Stearns M B 1976 *Phys. Rev.* B **13** 1183
Swanson M L, Howe L M and Quenneville A F 1980 *Nucl. Instrum. Meth.* **170** 427
Takaki S, Fuss J, Kugler H, Dedek U and Schultz H 1983 *Radiat. Eff.* **79** 87
Taylor A 1961 *X Ray Metallography* (New York: Wiley) p 340
Vanoni F 1973 *Thèse* Université de Grenoble
Vehanen A, Hautojärvi P, Johansson J, Yli-Kauppila J and Moser P 1982 *Phys. Rev.* B **25** 762
Walz F, Blythe H J and Dworschak F 1982 *Phys. Status Solidi* a **75** 235